

The Critical Density and the Effective Excitation Density of Commonly Observed Molecular Dense Gas Tracers

Yancy L. Shirley^{1,2}

ABSTRACT

The optically thin critical densities and the effective excitation densities to produce a 1 K km/s (or 0.818 Jy km/s $(\frac{\nu_{ik}}{100\text{GHz}})^2 (\frac{\theta_{beam}}{10''})^2$) spectral line are tabulated for 12 commonly observed dense gas molecular tracers. The dependence of the critical density and effective excitation density on physical assumptions (i.e. gas kinetic temperature and molecular column density) is analyzed. Critical densities for commonly observed dense gas transitions in molecular clouds (i.e. HCN 1 – 0, HCO⁺ 1 – 0, N₂H⁺ 1 – 0) are typically 1 – 2 orders of magnitude larger than effective excitation densities because the standard definitions of critical density do not account for radiative trapping and 1 K km/s lines are typically produced when radiative rates out of the upper energy level of the transition are faster than collisional depopulation. The use of effective excitation density has a distinct advantage over the use of critical density in characterizing the differences in density traced by species such as NH₃, HCO⁺, N₂H⁺, and HCN as well as their isotopologues; but, the effective excitation density has the disadvantage that it is undefined for transitions when $E_u/k \gg T_k$, for low molecular column densities, and for heavy molecules with complex spectra (i.e. CH₃CHO).

1. Introduction

The density at which a particular molecular transition is excited has always been an interesting quantity for studies of molecular gas in the interstellar medium. Two concepts have been developed, the critical density and the effective excitation density, to quantify the excitation density of a transition. A traditional approach in studying the critical density has been to consider the molecular rotational energy levels as a simple two level system. While this approach has pedagogical advantages, the interpretation of concepts, such as critical density, are oversimplified and incorrect. Molecules are fundamentally multi-level systems

¹Steward Observatory, 933 N Cherry Ave., Tucson, AZ 85721 USA

²Max-Planck-Institut für Astronomie (MPIA), Königstuhl 17, 69117, Heidelberg, Germany

with radiative and collisional processes between the levels (Figure 1). It is almost never appropriate to approximate commonly observed dense gas tracers, such as HCO^+ , HCN , NH_3 , N_2H^+ , etc., as two level systems. Therefore, in this tutorial, we eschew the two level approximation and consider the full multi-level nature of molecular excitation. It is assumed that the reader has a basic familiarity with statistical equilibrium, radiative transfer, and molecular spectroscopy. For a summary of radiative transfer techniques and molecular data used in those calculations, see van der Tak (2011) and references therein. The purpose of this tutorial is to quantify and systematize the use of critical density and effective excitation density for dense gas molecular tracers.

We shall use the excitation of two molecules, HCO^+ and NH_3 , as examples throughout this tutorial. Figure 1 shows the energy level structure for both molecules. HCO^+ is an abundant linear molecule with a simple $^1\Sigma$ electronic ground state meaning that there is zero net electronic spin and zero net electronic angular momentum that could interact with and split the rotational levels of the molecule. Electric dipole selection rules limit transitions to $\Delta J = \pm 1$. The $1-0$ ground state rotational transition is a millimeter transition at 89 GHz (3.3 mm) and the frequency of rotational transitions progress linearly into the submillimeter part of the spectrum.

NH_3 is an abundant pyramidal symmetric top molecule with a simple 1A_1 electronic ground state also meaning that there is zero net electronic spin and zero net electronic angular momentum. The energy levels are designed by J_K where J is the total rotational angular momentum and K is the projection of the angular momentum onto the NH_3 symmetry axis. Electric dipole transitions do not allow the projected angular momentum to change ($\Delta K = 0$). As a result, the energy level structure is usually organized in K-ladders with each K-ladder designated as either ortho ($K = 0, 3, 6$, etc.) or para ($K = 1, 2, 4, 5$, etc.) due to the spin symmetry required to satisfy Fermi-Dirac statistics for each rotational energy level. The plane of three H atoms can tunnel from positions above and below the N atom resulting in inversion splitting of each rotational level (with symmetry denoted by \pm) except for levels with $K = 0$ for which half of the inversion levels are missing due to the Pauli exclusion principle (see Townes & Schwalow 1975 for a detailed explanation). Electric dipole transitions are allowed between the inversion-split levels with different symmetries and these inversion transitions occur at wavelengths near 1.3 cm (24 GHz). Since J and K do not change in a pure inversion transition, the shorthand notation (J, K) has been adopted. As with HCO^+ , there are rotational transitions with $\Delta J = \pm 1$, but since NH_3 is a lighter molecule than HCO^+ ($E_{rot} \propto 1/I$ where I is the moment of inertia of the molecule measured from a coordinate system at the center-of-mass), the transitions occur at submillimeter and far-infrared wavelengths. Thus, the lowest energy transitions of HCO^+ and NH_3 cover a wide range of wavelengths from the centimeter to the far-infrared.

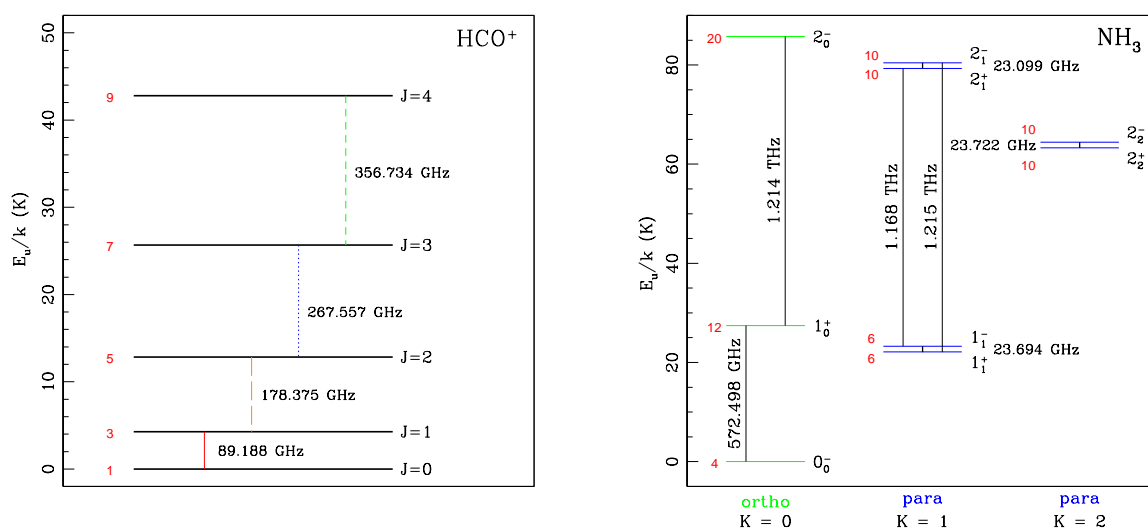


Fig. 1.— Left: The energy level structure for HCO⁺ showing the lowest 4 energy levels. Electric dipole allowed transitions are shown along with the quantum numbers (J) to the right of each level and statistical weights in red to the left of each energy level. Right: The energy level structure for NH₃ showing the lowest 9 energy levels. Electric dipole allowed transitions are shown along with the quantum numbers (J_K^\pm) to the right of each level and statistical weights in red to the left of each energy level. This figure was adapted from figures in Mangum & Shirley (2015).

2. Critical Density

The critical density has traditionally been used as a measure of the density at which a particular transition is excited and is observed at radio wavelengths. The definition of the critical density is not consistent throughout the literature. Some definitions only consider the two energy levels involved in the transition (2 level approximation) while other definitions use the multi-level nature of collisions to sum over all collisions out of the upper energy level or only from the upper energy level to lower energy levels. All of the standard definitions assume the molecular emission is optically thin and ignore radiative trapping which is very important and cannot be ignored for many commonly observed dense gas tracers (e.g. HCN $1 - 0$, HCO⁺ $1 - 0$, N₂H⁺ $1 - 0$, etc.; see §2.2). The standard definitions also usually ignore continuum backgrounds (see §4).

We start by defining the critical density as the density for which the net radiative decay rate from $j \rightarrow k$ equals the rate of collisional depopulation out of the upper level j for a multilevel system. The net radiative decay rate from $j \rightarrow k$ is the spontaneous decay rate from $j \rightarrow k$ plus the stimulated emission rate from $j \rightarrow k$ minus the absorption rate from $k \rightarrow j$. Mathematically, the ratio of rates is

$$\mathfrak{R} = \frac{n_j A_{jk} + n_j B_{jk} u_{\nu_{jk}} - n_k B_{kj} u_{\nu_{jk}}}{n_c n_j \sum_{i \neq j} \gamma_{ji}}, \quad (1)$$

where n_j is the number density (cm⁻³) of molecules in the upper level of the transition, n_k is the number density (cm⁻³) of molecules in the lower level of the transition, n_c is the number density (cm⁻³) of colliding particles (typically H₂, H, or e⁻), and γ_{ji} are the collision rates (cm³ s⁻¹) out of level j into another level i . n_c is equal to n_{crit} when $\mathfrak{R} = 1$. A_{jk} and B_{jk} are the Einstein A (s⁻¹) and B (erg⁻¹ cm³ s⁻²) coefficients related by

$$\frac{g_k}{g_j} B_{kj} = B_{jk} = \frac{c^3}{8\pi h \nu_{jk}^3} A_{jk} \quad . \quad (2)$$

$u_{\nu_{jk}}$ is the energy density (erg cm⁻³ Hz⁻¹) of the radiation fields at the frequency of the transition ν_{jk} . The energy density is written in terms of a Planck function and is related to the angle and polarization averaged photon occupation number, n_{ph} , by

$$u_{\nu}(T) = \frac{8\pi h \nu^3}{c^3} \frac{1}{e^{h\nu/kT} - 1} = \frac{8\pi h \nu^3}{c^3} n_{ph}(T, \nu) \quad . \quad (3)$$

The total energy density can include contributions from the cosmic microwave background (CMB), dust continuum emission from the interstellar radiation field, dust continuum emission local to the molecular cloud, optically thick molecular emission at the frequency ν_{jk} , and other continuum and spectral line sources.

2.1. Optically Thin Approximation

We define the optically thin critical density without a background by solving for n_c in Equation 1 when $\mathfrak{R} = 1$ and ignoring the stimulated emission and absorption terms:

$$n_{crit}^{thin,no\ bg} = \frac{A_{jk}}{\sum_{i \neq j} \gamma_{ji}} = \frac{A_{jk}}{\sum_{i < j} \gamma_{ji} + \sum_{i > j} \frac{g_i}{g_j} \gamma_{ij} e^{-(E_i - E_j)/kT_k}} . \quad (4)$$

The sum over collision rates in the denominator of Equation 4 has been split in two terms depending on whether the collision from level j is to an energy level lower in energy (first sum) or higher in energy (second sum) than level j . Upward collision rates are related to downward collision rates using detailed balance by

$$\gamma_{ji} = \gamma_{ij} \frac{g_i}{g_j} e^{-(E_i - E_j)/kT_k} \quad \text{for } E_i > E_j \quad (5)$$

where T_k is the kinetic temperature of the collisional partner. Published collision rates (i.e. the Leiden molecular database¹; Schöier et al. 2005) quote only downward collision rates. In the two level approximation, which is widely quoted but rarely appropriate, the sums reduce to a single term such that $n_{crit,2lvl}^{thin,no\ bg} = \frac{A_{jk}}{\gamma_{jk}}$. As a result, $n_{crit,2lvl}^{thin,no\ bg}$ will always be larger (usually by at least a factor of a few) than $n_{crit}^{thin,no\ bg}$.

It is instructive to compare how the optically thin critical density compares to the excitation temperature. For a particular transition between levels $j \rightarrow k$, the level population are related to the excitation temperature, T_{ex} , between the two levels by Boltzmann's equation

$$\frac{n_j}{n_k} = \frac{g_j}{g_k} \exp\left(-\frac{E_j - E_k}{kT_{ex}}\right) \quad \text{for } E_j > E_k . \quad (6)$$

The excitation temperature (and therefore the level populations) depend on the density of colliding partners (n_c), the gas kinetic temperature of colliding partners (T_k), and the energy density of radiation fields that the molecules are exposed to. The dependence of T_{ex} on the density and gas kinetic temperature for the ground state transitions of ortho and para NH_3 are shown in Figure 2. The only background radiation field assumed in this example is the CMB. At low densities ($n_c < 10^3 \text{ cm}^{-3}$), the level populations come into equilibrium with the CMB and T_{ex} approaches $T_{cmb} = 2.725 \text{ K}$. As the density increases, collisions become more important in determining the level populations. The excitation temperature of (1, 1) centimeter wavelength inversion transition equilibrates to T_k by densities $> 10^{5.5} \text{ cm}^{-3}$ while the submillimeter $1_0 - 0_0$ rotational transition equilibrates to T_k at significantly higher

¹<http://home.strw.leidenuniv.nl/~moldata/>

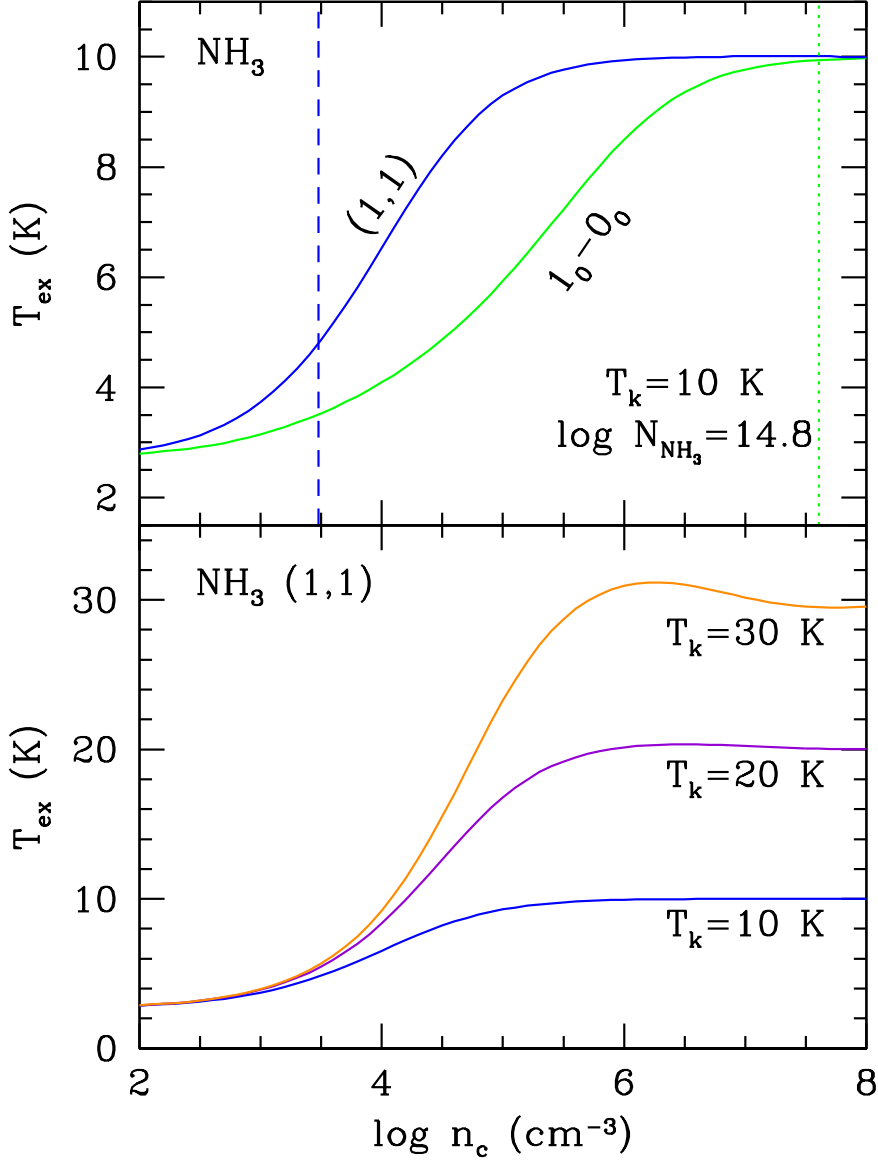


Fig. 2.— Top: The excitation temperature is plotted for the NH₃ (1,1) inversion transition (23.7 GHz, 1.3 cm) and $1_0 - 0_0$ rotational transition (572.5 GHz, 0.52 mm) for a gas kinetic temperature of 10K and a total NH₃ reference column density of $\log N = 14.8 \text{ cm}^{-3}$ (an ortho to para ratio of 2 : 1 is assumed). The blue dashed line and the green dotted line indicate $n_{\text{crit}}^{\text{thin, no bg}}$ for the (1,1) and $1_0 - 0_0$ transitions respectively. Bottom: The variation of excitation temperature for the NH₃ (1,1) transition with gas kinetic temperature is plotted for $T_k = 10, 20,$ and 30 K .

densities ($> 10^7 \text{ cm}^{-3}$). The general shape of the T_{ex} with $\log n_c$ curves is a sigmoid curve with stimulated coupling with the background radiation field setting the lower bound at low densities and collisions with colliding partners at T_k setting the upper bound. At densities where $T_{ex} < T_k$, the level populations are said to be sub-thermally populated. This is the situation for most of the commonly observed dense gas transitions in the ISM. When T_{ex} approaches T_k , the level populations are said to be thermalized.²

At optical wavelengths (the high frequency limit), critical density is interpreted as the density at which an atomic forbidden line is quenched by collisions meaning that a collisional de-excitation occurs before a photon can be generated from spontaneous emission. In the optical, quenching occurs when T_{ex} is thermalized ($T_{ex} \rightarrow T_k$). At radio wavelengths (the low frequency limit) the critical density occurs at different positions along the sigmoid T_{ex} curve for different molecular tracers and different transitions. In the case of the 1.3 cm (23.7 GHz) NH_3 (1,1) transition, the optically thin critical density is two orders of magnitude below the thermalization density (Figure 2). Early radio astronomy observations of molecules such as OH and NH_3 occurred at centimeter wavelengths and since the critical density at these low frequencies is just above the regime where the T_{ex} starts to rise above equilibration with the CMB, critical density was used to indicate the density at which a transition would appear in emission. As the frequency of the transition increases, the critical density moves farther up the T_{ex} curve. For the 0.52 mm (572 GHz) NH_3 $1_0 - 0_0$ transition, the critical density is nearly equal to the density required for thermalization. Millimeter transitions are an intermediate case; thus, neither the radio interpretation of critical density being the density at which an emission line is excited nor the optical interpretation of critical density being the density at which an emission line is quenched is appropriate.

2.2. Optically Thick Emission

In reality, radiative trapping is very important for many molecular transitions observed in the dense interstellar medium and cannot be ignored. The energy density is then modified using the solution to the equation of radiative transfer to include emission from the molecule at the excitation temperature describing the level populations for a transition from $j \rightarrow k$

²Note that the T_{ex} curve for NH_3 (1,1) shows a region of super-thermal excitation ($T_{ex} > T_k$) at densities immediately before thermalization for the $T_k = 30 \text{ K}$ curve. This is due to a bottleneck in radiative transitions, caused by the five orders of magnitude difference between the spontaneous emission rates for the inversion transition and the THz rotational transition into the upper inversion level, resulting in a slight overpopulation of the upper level of the inversion transition. This effect is more pronounced for higher T_k because upward collisions to the $J_K = 2_1$ levels are more efficient at high T_k (see Equation 5).

as

$$u_{\nu_{jk}} = u_{\nu_{jk}}(T_{bg})\bar{\beta} + u_{\nu_{jk}}(T_{ex})(1 - \bar{\beta}) \quad , \quad (7)$$

where $\bar{\beta}$ is the solid angle averaged escape fraction (see Chapter 19 of Draine 2011 for a derivation). If we multiply the energy density by the conversion factor between Einstein B_{jk} and A_{jk} terms from Equation 2, then we find that

$$\frac{c^3}{8\pi h\nu_{jk}^3}u_{\nu_{jk}} = n_{ph}(T_{bg}, \nu_{jk})\bar{\beta} + n_{ph}(T_{ex}, \nu_{jk})(1 - \bar{\beta}) \quad . \quad (8)$$

In the limit that the background radiation can be ignored ($u_{\nu_{jk}}(T_{bg})\bar{\beta} \ll u_{\nu_{jk}}(T_{ex})(1 - \bar{\beta})$), the critical density becomes

$$\begin{aligned} n_{crit}^{thick, no\ bg} &= \frac{n_j A_{jk} + n_j A_{jk} n_{ph}(T_{ex}, \nu_{jk})(1 - \bar{\beta}) - n_k \frac{g_j}{g_k} A_{jk} n_{ph}(T_{ex}, \nu_{jk})(1 - \bar{\beta})}{n_j \sum_{i \neq j} \gamma_{ji}} \\ &= \frac{n_j A_{jk} \left[1 + (1 - \frac{g_j}{g_k} \frac{n_k}{n_j}) n_{ph}(T_{ex}, \nu_{jk})(1 - \bar{\beta}) \right]}{n_j \sum_{i \neq j} \gamma_{ji}} \\ &= \frac{A_{jk} \left[1 + (\frac{-1}{n_{ph}(T_{ex}, \nu_{jk})}) n_{ph}(T_{ex}, \nu_{jk})(1 - \bar{\beta}) \right]}{\sum_{i \neq j} \gamma_{ji}} \\ &= \frac{\bar{\beta} A_{jk}}{\sum_{i \neq j} \gamma_{ji}} \quad . \quad (9) \end{aligned}$$

Comparing Equation 9 with Equation 4, we see that the effect of radiative trapping is to reduce the spontaneous transition rate by the escape fraction $\bar{\beta} A_{jk}$ (see Scoville & Solomon 1974, Goldreich & Kwan 1974).

The relationship between $\bar{\beta}$ and the line of sight optical depth, $\tau_{\nu_{jk}}$, depends on the geometry and kinematics of the region. In the case of a static, uniform density sphere

$$\bar{\beta} = \frac{3}{4\tau_{\nu_{jk}}} - \frac{3}{8\tau_{\nu_{jk}}^3} + e^{-2\tau_{\nu_{jk}}} \left(\frac{3}{4\tau_{\nu_{jk}}^2} + \frac{3}{8\tau_{\nu_{jk}}^3} \right) \quad (10)$$

(Osterbrock 1989), while in the case of a spherical cloud with a large velocity gradient $v \propto r$ (the LVG or Sobolev approximation),

$$\bar{\beta} = \frac{(1 - e^{-\tau_{\nu_{jk}}})}{\tau_{\nu_{jk}}} \quad (11)$$

(Sobolev 1960, Castor 1970). For large optical depths ($\tau_{\nu_{jk}} \gg 5$), the effective spontaneous transition rate is then given by $\bar{\beta} A_{jk} \sim A_{jk}/\tau_{\nu_{jk}}$.

This result has an important effect on the critical density by reducing its value from the optically thin value. The most commonly observed transition of molecular gas is ^{12}CO $1 - 0$. The optically thin critical density at $T_k = 10$ K is $n_{crit}^{thin, no\ bg} = 1 \times 10^3 \text{ cm}^{-3}$; however, since ^{12}CO $1 - 0$ has optical depths that are typically more than a factor of 10 in molecular clouds (and usually much higher), it is easy to observe strong lines (> 1 K km/s) in gas that has densities $< 10^2 \text{ cm}^{-3}$. Optical trapping is so important for CO that it does not make sense to use the optically thin critical density.

Commonly observed lines of dense gas tracers in cores and clumps also tend to be optically thick. The upper left panel of Figure 3 shows the predicted optical depth of HCO^+ $1 - 0$ through $4 - 3$ at different densities from a simple (single density, single temperature) radiative transfer model predicting that these transition are expected to be very optically thick over a wide range of densities. Observations support this prediction. For example, several hundred high-mass clumps mapped in the MALT90 Galactic survey have a median optical depth of $\tau = 23$ for the HCO^+ $1 - 0$ transition (Hoq et al. 2013). Clumps observed in the Bolocam Galactic Plane Survey (BGPS) in the higher frequency transition HCO^+ $3 - 2$ have an average $\tau = 10$ (Shirley et al. 2013). As a result, the analytically calculated critical densities using the optically thin approximation (Equation 4) are systematically biased toward higher densities by an order of magnitude or more. HCO^+ is not unique as most commonly observed dense gas tracers (i.e. HCN, CS, N_2H^+ , etc.) in the dense, cold neutral medium are typically both sub-thermally populated ($T_{ex} < T_k$) and optically thick (also see Plume et al. 1997, Gerner et al. 2014). In practice, to properly estimate the optical depth, a coupled radiative transfer and statistical equilibrium calculation must be performed to find the level populations upon which the optical depth depends (since $\tau_{\nu_{jk}} \propto \int (n_k B_{kj} - n_j B_{jk}) ds$ along the line-of-sight s). Since the escape fraction depends nonlinearly with column density (for modest optical depths), nonlinearly with geometry, and nonlinearly with gas kinetic temperature, it is difficult to make a simple tabulation of a $\bar{\beta}$ correction to $n_{crit}^{thin, no\ bg}$.

3. Effective Excitation Density

It is possible to detect strong (1 K km/s) molecular lines at densities well below the critical density (see Figure 3). An alternative definition has been developed to trace the effective density at which a modest line intensity is observed that is based on radiative transfer calculations with reasonable assumptions about the column density and gas kinetic temperature of the region (Evans 1999). The effective excitation density is defined as

$$n_{eff} = n_c \ni \int T_R dv = 1 \text{ K km/s} \quad , \quad (12)$$

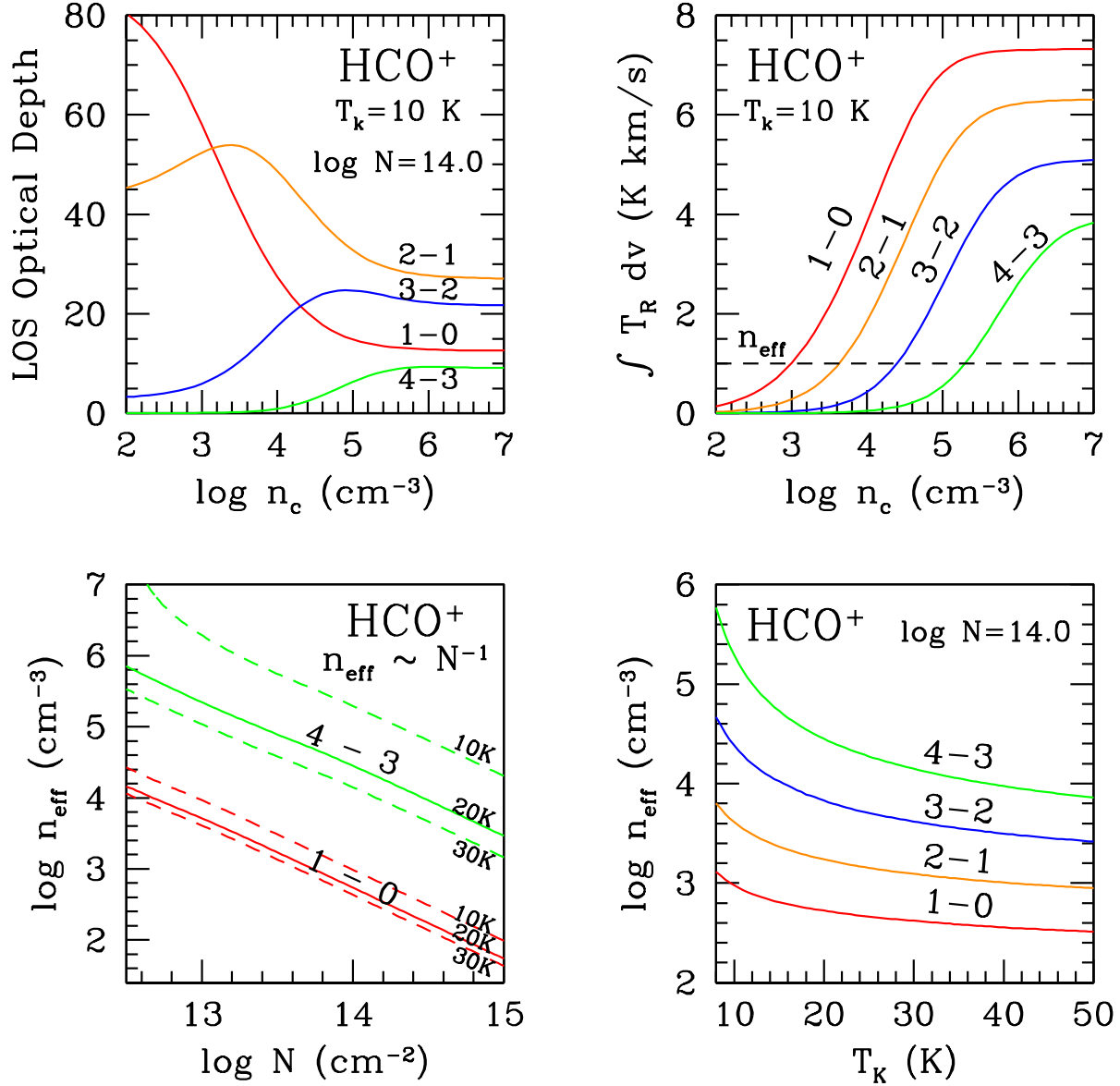


Fig. 3.— Top Left: Line of sight optical depth for HCO⁺ transitions. A column density of $\log N = 14.0$ and a gas kinetic temperature of $T_k = 10$ K were assumed. Top Right: The integrated intensity for HCO⁺ transitions. A column density of $\log N = 14.0$ and a gas kinetic temperature of $T_k = 10$ K were assumed. The horizontal dashed line is the criterion for the definition of n_{eff} used in this paper. Bottom Left: n_{eff} is inversely proportional column density. Only the HCO⁺ 1-0 and 4-3 transitions are shown for clarity. The solid line is calculated at $T_k = 20$ K while the dashed lines above and below the solid line correspond to $T_k = 10$ K and $T_k = 30$ K. Bottom Right: The dependence of n_{eff} on choice of gas kinetic temperature for the four lowest rotational transitions of HCO⁺. n_{eff} was calculated assuming the reference column density of $\log N = 14.0$.

the density which results in a molecular line with an integrated intensity of 1 K km/s. The choice of 1 K km/s is arbitrary but represents an easily detectable integrated intensity³. For lower integrated intensity criteria, n_{eff} decreases (Figure 3). It is important to note that the effective excitation density is based on a simple empirical criterion and is not based on $\mathfrak{R} = 1$ or any specific ratio of radiative rates to collisional depopulation rates. n_{eff} does however account for the effects of radiative trapping. The original definition presented in Evans (1999) defined n_{eff} as the density resulting in $T_R = 1$ K line and used a LVG radiative transfer code to calculate n_{eff} . We shall use the radiative transfer code RADEX (van der Tak et al. 2007) with the escape probability formalism for a static, uniform density sphere, with the CMB as the only background radiation field, and with H₂ as the dominant collision partner for all calculations. The definition in Equation 12 is approximately equivalent to the Evans 1999 definition when a FWHM linewidth of 1 km/s is assumed in RADEX calculations.

3.1. Properties of Effective Excitation Density

The column density of the observed molecule and the gas kinetic temperature of the colliding partner must be assumed in order to calculate n_{eff} . The sensitivity of n_{eff} to these assumptions is explored in Figure 3 for the HCO⁺ molecule. At lower column densities, a higher n_{eff} is required to produce a 1 K km/s line. As the column density increases by an order of magnitude, the n_{eff} decreases by almost exactly an order of magnitude. The effective excitation density is inversely proportional to column density

$$n_{eff}(T_k, N) \approx n_{eff}(T_k, N_{ref}) \frac{N_{ref}}{N} \quad , \quad (13)$$

where N_{ref} is a reference column density. This simple scaling proportionality breaks down for $n_{eff} \gtrsim 5 \times 10^6 \text{ cm}^{-3}$ and the relationship between n_{eff} and N becomes noticeably non-linear (see the $T_k = 10$ K curve for HCO⁺ 4 – 3 in the bottom left panel of Figure 3). In those cases, a new RADEX model should be run to scale tabulated results to a new column density.

The dependence of n_{eff} to T_k is nonlinear and more sensitive at low kinetic temperatures ($T_k < 20$ K) due to the inefficiency of upward collisions at lower T_k (Figure 3). An order of magnitude higher n_{eff} is required to make a 1 K km/s line for $T_k = 10$ K than at $T_k = 30$ K for HCO⁺ 3 – 2. This sensitivity is due to the exponential dependence from upward

³The radiation temperature is related to the observed flux density $S_{\nu_{jk}}$ through $T_R = \frac{c^2}{2k\nu_{jk}^2 \Omega_{beam}} S_{\nu_{jk}}$ where $\Omega_{beam} = \frac{\pi \theta_{beam}^2}{4 \ln 2}$ is the solid angle of the telescope beam with FWHM θ_{beam} . A 1 K km/s integrated intensity corresponds to an integrated flux density of $0.818 \text{ Jy km/s} \left(\frac{\nu_{jk}}{100\text{GHz}}\right)^2 \left(\frac{\theta_{beam}}{10''}\right)^2$.

collisional rates (Equation 4) and becomes more pronounced when the upper energy level is significantly higher than T_k (i.e. the effect is stronger for $4 - 3$ vs. $1 - 0$ at $T_k < 20$ K because $E_u/k = 42.8$ K for $J = 4$ vs. $E_u/k = 4.3$ K for $J = 1$).

Table 1 gives n_{eff} for 12 dense gas tracers at $T_k = 10, 15, 20, 50,$ and 100 K for a reference column density. Recent surveys of dense gas in the Milky Way may be used to guide our choice of the reference column density. For example, observations of several hundred clumps by the MALT90 (Meitinen et al. 2013, Hoq et al. 2013), ChaMP (Barnes et al. 2012), and BGPS (Shirley et al. 2013) surveys indicate that HCO^+ column densities typically span from $\log N = 12 - 15.5$. The Hoq et al. and Shirley et al. surveys find median column densities of clumps drawn from the ATLASGAL and BPGS Galactic plane surveys that are in agreement near $\log(\text{med}\{N\}) = 14.4$. Miettenen’s (2014) analysis of infrared dark clouds (IRDCs) indicates a significantly lower median column density of $\log(\text{med}\{N\}) = 13.1$. All of these surveys use observations of H^{13}CO^+ to correct the optical depth of the HCO^+ line. The Barnes et al. (2011) blind mapping survey of a section of the southern Galactic plane find a smaller value of $\log(\text{med}\{N\}) = 12.9$, but did not observe H^{13}CO^+ to make optical depth corrections. We chose a column density that is intermediate between the IRDC, low-mass samples, and the Galactic plane surveys of $\log(N_{ref}) = 14.0$. For comparison, Evans (1999) tabulate the effective density for HCO^+ assuming $\log N = 13.5$.

The reference column densities for each molecule in Table 1 are estimated from surveys in dense gas tracers (Suzuki et al. 1992, Zylka et al. 1992, Mangum & Wootten 1993, Plume et al. 1997, Jijina et al. 1999, Savage et al. 2002, Pirogov et al. 2003, Purcell et al. 2006, Blair et al. 2008, Rosolowsky et al. 2008, Falgarone et al. 2008, Hily-Blant et al. 2010, Barnes et al. 2011, Dunham et al. 2011, Ginsburg et al. 2011, Reiter et al. 2011, Adande et al. 2012, Benedettini et al. 2012, Wienen et al. 2012, Hoq et al. 2013, Shirley et al. 2013, Gerner et al. 2014, Miettenen et al. 2014 Yuan et al. 2014). Since these surveys contain many biases (i.e. only study massive high-mass regions or only study nearby low-mass regions, etc.), N_{ref} represents an educated guess at a typical value intermediate between high-mass clumps and low-mass cores. The tabulated n_{eff} can be easily scaled to another column density using Equation 13. ^{13}C isotopologue column densities assume no fractionation and an isotope ratio of $[^{12}\text{C}]/[^{13}\text{C}] = 50$, appropriate for a source in the Molecular Ring (Wilson & Rood 1994). For molecules with ortho and para states, LTE statistical equilibrium was assumed (2 : 1 ortho to para ratio for NH_3 and 3 : 1 ortho to para ratio for H_2CO).

3.2. Comparing Critical Density and Effective Excitation Density

The panels of Figure 4 summarize the range in $n_{crit}^{thin,no\ bg}$ and n_{eff} of commonly observed molecular tracers of dense gas for reference observed column densities and a gas kinetic temperature of $T_k = 15$ K. This temperature was chosen to be intermediate between the typical temperature of nearby low-mass cores (10 K, Jijina et al. 1999, Rosolowsky et al. 2008, Seo et al. 2015, submitted) and high-mass clumps in the Galactic plane (20 K, Dunham et al. 2011, Wielen et al. 2012). n_{eff} is lower than $n_{crit}^{thin,no\ bg}$ in nearly all cases by 1–2 orders of magnitude. This is partially due to the sensitivity of n_{eff} to line trapping in optically thick transitions. Transitions that are the most optically thick have the largest average $n_{crit}^{thin,no\ bg}/n_{eff}$ ratios (i.e 121 for HCO⁺ transitions and 88 for HCN transitions where the average is calculated for 1–0 through 4–3 transitions). Less optically thick species have smaller ratios (i.e. average ratios of 16 for CN and 10 for N₂H⁺). The species plotted with the smallest difference between $n_{crit}^{thin,no\ bg}$ and n_{eff} is the optically thin isotopologue H¹³CN with an average ratio of 1.7. Some heavier species whose transitions are likely close to optically thin listed in Table 1 also have low average ratios that are less than 3 (i.e. H₂CO, HC₃N, and CH₃CN). These results indicate that a 1 K km/s line is typically observed for transitions when $\mathfrak{R} > 1$ in Equation 1 or when the radiative rates are greater than collisional depopulation out of the upper energy level of the transition.

There is also typically an increase in $n_{crit}^{thin,no\ bg}$ and n_{eff} with J_u for a particular molecule (Figure 4). This behavior can be understood from the functional dependences on A_{jk} and γ_{jk} in Equation 4 ($n_{crit}^{thin,no\ bg} \sim A_{jk}/\gamma_{jk}$). The Einstein A for electric dipole allowed transitions is $A_{jk} \propto \mu_e^2 \nu_{jk}^3$, where μ_e is the molecular permanent electric dipole moment. In general, molecules with larger μ_e will trace denser gas. For instance, $\mu_e = 2.99$ D for HCN while $\mu_e = 0.11$ D for CO (Ebenstein & Muentner 1984, Goorvitch 1994), partially explaining why HCN is a denser gas tracer than CO (the other effect being that the optical trapping in ¹²CO lines is often very large; see §2.2). Since $\nu_{jk} \propto J_u$ and the Einstein A_{jk} has a ν_{jk}^3 dependence, higher frequency transitions of a particular molecule will trace higher densities. This statement is also true for comparing molecules with similar permanent electric dipole moments but with transitions at different frequencies. As an example, the frequency of the NH₃ ($\mu_e = 1.47$ D; Ueda & Iwahori 1986) inversion transitions (J,K=J) are nearly a factor of 4 lower than for the 1–0 transitions of HCO⁺ N₂H⁺ and HCN, thus the spontaneous transition rate is more than 60 times smaller, lowering the critical densities of NH₃ (1,1) with respect to the 1–0 transitions of HCO⁺ N₂H⁺ and HCN. One problem with the use of n_{crit}^{thin} becomes apparent for the NH₃ inversion transitions. Since NH₃ (1,1) through (4,4) are at nearly the same frequency (23.7 to 24.1 GHz), their $n_{crit}^{thin,no\ bg}$ are nearly identical. n_{eff} is sensitive to both line trapping and E_u/k of the transition resulting in an increase in n_{eff} for NH₃ (1,1) and (2,2) (N.B. n_{eff} for NH₃ (3,3) and (4,4) are undefined at $T_k = 15$ K as we

will discuss below).

Differences in collision rates also affect the ranking of molecules with density in Figure 4. HCN is observed to have 1 - 2 orders of magnitude higher $n_{crit}^{thin, no\ bg}$ and n_{eff} than HCO^+ . Both HCO^+ and HCN transitions have similar A_{jk} values, but HCO^+ is an ion and the collisional cross section for collisions with H_2 is larger than for neutral species (see Flower 1999 vs. Dumouchel et al. 2010). This reduces the critical density and effective excitation density of HCO^+ relative to HCN.

The ordering of species with increasing density is different for $n_{crit}^{thin, no\ bg}$ versus n_{eff} among many of the molecules plotted in Figure 4. A problem with using $n_{crit}^{thin, no\ bg}$ can be seen when HCO^+ and N_2H^+ are compared. HCO^+ and N_2H^+ are both ions with similar A_{jk} values for transitions and similar collisional cross-sections and thus have similar $n_{crit}^{thin, no\ bg}$; however, it is common knowledge to observers of nearby, low-mass dense cores that N_2H^+ is a denser gas tracer than HCO^+ . Due to chemical effects, N_2H^+ typically has lower abundance and therefore lower column density than HCO^+ resulting in a higher n_{eff} (see Equation 13).

n_{eff} also does a better job than $n_{crit}^{thin, no\ bg}$ of characterizing the difference in density traced by isotopologues versus the main species. The ratio of A_{jk} for the $1 \rightarrow 0$ transition between H^{13}CN and HCN is 0.92. This accounts for the slightly lower $n_{crit}^{thin, no\ bg}$ for H^{13}CN versus HCN; however, we know that the isotopologues should trace higher density gas than the main species because it is more optically thin and has a lower column density (see Equation 13). The average ratio of n_{eff} for $\text{H}^{13}\text{CN}/\text{HCN}$ $1 \rightarrow 0$ is 41 ($T_k \in [10, 100]$ K). This ratio is not exactly equal to the assumed isotope ratio and column density ratio of 50 because of differences in A_{jk} , collisional rates, and line trapping between the isotopologue and main species.

These examples illustrates important advantages in using n_{eff} rather than the critical density; however, using n_{eff} has a significant disadvantage in that n_{eff} is undefined when an integrated intensity of 1 K km/s cannot be observed. This is the case for the NH_3 (3,3) ($E_u/k = 123.5$ K) and higher inversion lines at low gas kinetic temperature. When $E_u/k \gg T_k$, the upper energy state cannot attain a high enough population to result in large enough radiative rates to produce a 1 K km/s line. High J_u transitions for species such as NH_3 , HCN, HCO^+ , and N_2H^+ will be undefined at low gas kinetic temperatures ($T_k \lesssim 20$ K).

Another problem with the standard definition of n_{eff} is that the more complex the spectrum of a molecule (e.g. a heavy asymmetric top molecule), the less likely a particular transition will attain enough level population to produce a 1 K km/s emission line. For instance, no transitions of HNCO have intensities greater than 1 K km/s for the observed

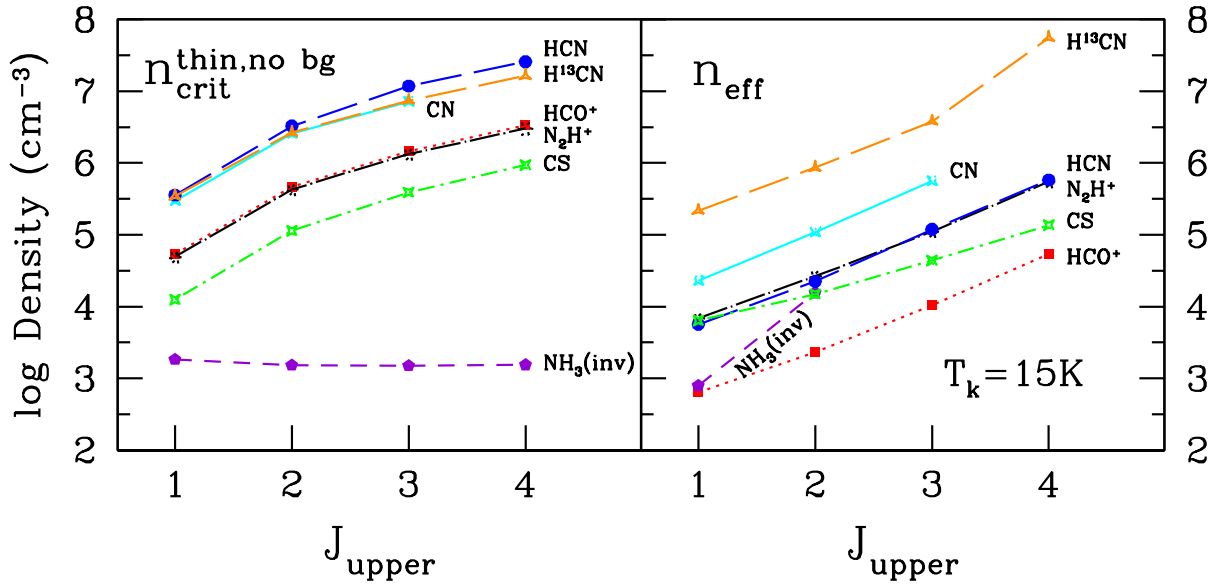


Fig. 4.— Left: $n_{crit}^{thin,no bg}$ calculated at $T_k = 15$ K for popular dense gas tracers. Each point corresponds to the upper state rotational quantum number J of the transition. The ordering of labels correspond to the ordering of the curves in increasing density for each molecule. Note that the curves for HCO^+ and N_2H^+ nearly overlap as well as for CN and H^{13}CN . Right: n_{eff} calculated for $T_k = 15$ K and at the reference column density determined from surveys of Galactic sources (see Table 1). Note that the curves for HCN and N_2H^+ nearly overlap. The critical density is typically one to two orders of magnitude above n_{eff} for these tracers.

median column density of $\log \text{med}\{N\} = 12.6$ (Gerner et al. 2014). n_{eff} for complex organic species (i.e. CH_3CHO , CH_3OCH_3 , etc.) will be undefined. One solution is to reduce the 1 K km/s criterion, Ultimately, the choice for this criterion is arbitrary, but unless all researchers agree to use the same criterion, n_{eff} could not be compared among different papers and for different species. The upper right panel of Figure 3 shows the non-linear sensitivity of the integrated intensity for different transitions of HCO^+ with density. As the integrated intensity criterion is lowered, the curves flatten with n_c indicating that a smaller decrease in the criterion results in a larger decrease in n_{eff} . These problems limit the utility of n_{eff} compared to $n_{crit}^{thin,no\ bg}$ which can always be calculated if collision rates are known.

4. A Caveat About Continuum Radiation Backgrounds

We ignored continuum background radiation fields in §2 when deriving the expressions for $n_{crit}^{thin,no\ bg}$ and $n_{crit}^{thick,no\ bg}$, while only the CMB was considered as a background in the RADEX models in §3. In this section we consider when contributions from the CMB and dust continuum background are important.

The ratio of the rate of stimulated emission from $j \rightarrow k$ due to the CMB to spontaneous emission is given by

$$\frac{B_{jk}u_{\nu_{jk}}(T_{cmb})}{A_{jk}} = \frac{1}{e^{h\nu_{jk}/kT_{cmb}} - 1} = n_{ph}(T_{cmb}, \nu_{jk}) . \quad (14)$$

This ratio is 2 for the NH_3 (J,K=J) inversion transitions and is a modest 0.26 at 90 GHz (3.3 mm), near the frequency of the fundamental transitions of commonly observed dense gas tracers (e.g. HCO^+ , HCN , HNC , N_2H^+). This ratio drops below 0.1 for transitions with $\nu_{jk} > 140$ GHz ($\lambda_{jk} < 2.1$ mm). Table 1 lists $n_{ph}(T_{cmb}, \nu_{jk})$ for each transition. For low frequency (long wavelength) transitions, stimulated emission and absorption due to the CMB should not be ignored.

Interesting examples of the interaction of low frequency transitions with the CMB are the K-doublet transitions of ortho- H_2CO ($1_{1,0} - 1_{1,1}$, $2_{1,1} - 2_{1,2}$, etc.). The 4.6 GHz (6.5 cm) $1_{1,0} - 1_{1,1}$ transition has a stimulated emission rate to spontaneous emission rate ratio of 11.3. Since the statistical weights of the two level are identical, the absorption rate from the lower level is identical to the stimulated emission rate from the upper level. This line is typically observed in absorption for densities $n \lesssim 10^5 \text{ cm}^{-3}$ (Mangum et al. 2008). The absorption is created by the lowest energy level ($1_{1,1}$) having a collisionally-induced overpopulation that results in absorption against the CMB ($T_{ex} < T_{cmb}$) over a wide range of physical conditions (Evans 1975, Garrison 1975). The calculation of $n_{crit}^{thin,no\ bg}$ gives a ridiculously low value of

13 cm^{-3} at $T_k = 10 \text{ K}$. Clearly in cases such as these, the simple definition of critical density fails and more sophisticated radiative transfer and statistical equilibrium calculations that include the CMB background are required.

In addition to the CMB, dust continuum backgrounds from the Galactic interstellar radiation field and from emission local to the cloud can be important in modifying the level populations. The main effect of dust continuum emission on our definition of critical density is to introduce a new stimulated rate out of level j to higher energy levels, i . The energy density is now the energy density for optically thin dust emission

$$u_{\nu_{ij}}^{dust}(T_{dust}) = \tau_{\nu_{ij}}^{dust} u_{\nu_{ij}}(T_{dust}) \quad , \quad (15)$$

where $\tau_{\nu_{ij}}^{dust}$ is the dust optical depth at the frequency of the $i \rightarrow j$ transition and T_{dust} is the isothermal dust temperature (see Equation 4 of Shirley et al. 2011 for a derivation of the equivalent isothermal dust temperature at a given frequency in sources with density and temperature gradients). We only need to consider transitions between $i \rightarrow j$ that are allowed by electric dipole selection rules because the Einstein B_{ji} for absorption of $j \rightarrow i$ is directly proportional to the Einstein A_{ij} for spontaneous emission of $i \rightarrow j$ (see Equation 2). For many simple molecules (HCO^+ , N_2H^+ , HCN , CS , NH_3 , etc.) there is only one electric dipole permitted transition from j into the upper state i that needs to be considered. The ratio of the rate at which this absorption from $j \rightarrow i$ occurs to the spontaneous rate for the original $j \rightarrow k$ transition is

$$\begin{aligned} \frac{B_{ji} u_{\nu_{ij}}^{dust}}{A_{jk}} &= \frac{g_i A_{ij}}{g_j A_{jk}} \frac{\tau_{\nu_{ij}}^{dust}}{\exp(h\nu_{ij}/kT_{dust}) - 1} \\ &= \frac{g_i A_{ij}}{g_j A_{jk}} \mu m_{\text{H}} N_{\text{H}_2} \kappa_{\nu_{jk}} n_{ph}(T_{dust}, \nu_{ij}) \quad , \end{aligned} \quad (16)$$

where $\mu = 2.8$ is the mean mass per H_2 molecule (see Kauffmann et al. 2008), N_{H_2} is the H_2 column density (cm^{-2}), and $\kappa_{\nu_{jk}}$ is dust opacity (cm^2/gram of gas) at the frequency of the $j \rightarrow i$ absorption. The ratio of rates in Equation 16 is linear proportional to the H_2 column density and increases non-linearly with dust temperature.

For the following examples, we calculate the ratio of rates in Equation 16 assuming a H_2 column density of 10^{22} cm^{-3} (corresponding to $A_V \sim 10 \text{ mag}$), a gas mass to dust mass ratio of 100 : 1, and Ossenkopf & Henning opacities for coagulated grains with thin ice mantles (OH5, Ossenkopf & Henning 1994) that are appropriate for dense cores. For the NH_3 (1,1) transition, the upper level is radiatively coupled to the $J = 2, K = 1$ level via a 1.168 THz (267 μm) far-infrared transition (see Figure 1). If NH_3 is bathed in a dust continuum of 10 K, the stimulated rate of absorption out of the upper inversion level is four times the spontaneous rate of the (1,1) transition. This high ratio is partially driven by the ratio of

spontaneous rates between the terahertz transition and the centimeter inversion transition which is $A_{ij}/A_{jk} = 7.2 \times 10^5$. The net effect is that n_{eff} becomes larger as the energy density from dust continuum increases. When the upper level of a low frequency transition is radiatively coupled to far-infrared transitions, the absorption from dust continuum is an important rate that should not be ignored. This is the case for the centimeter transitions of molecules such as NH_3 , OH , and CH .

The effects of dust continuum radiation are significantly less for the lowest energy transitions of simple linear molecules. For the 267.5 GHz (1.1 mm) HCO^+ 3 – 2 transition at 10 K, the ratio of rates is 6×10^{-4} . At 50 K, the ratio of rates rises to a meager 7×10^{-3} . These very low ratios indicate that the absorption due to dust continuum emission is not important for the level populations associated with millimeter transitions of linear molecules such as HCO^+ , HCN , CS , and N_2H^+ .

We have only considered the rotational levels of the molecule, but there can also be coupling between the radiation field and vibrational levels or electronic levels of the molecule that can effect the level populations of the ground vibrational state rotational levels. A mid-infrared continuum can pump the molecule from the ground vibrational state into an excited vibrational state which then radiatively decays via ro-vibrational transitions. For example, the HCN and HNC molecules have bending modes ($\nu_1, \nu_2, \nu_3 = 0, 1, 0$) that can be excited by mid-infrared pumping at 14 μm and 21 μm respectively. In environments where such pumping may be important (i.e. the inner envelope of high-mass protostars or near an AGN), the level populations can be affected by mid-infrared pumping. In these cases, more sophisticated radiative transfer models are needed.

5. Summary

In this tutorial, $n_{crit}^{thin, no\ bg}$ and n_{eff} are defined and their properties analyzed. The values for $n_{crit}^{thin, no\ bg}$ and n_{eff} are calculated for multiple transitions of 12 commonly observed dense molecular gas species in Table 1. n_{eff} inversely depends on the choice of column density and increases non-linearly as gas kinetic temperatures are lowered ($T_k < 20$ K). We have estimated the reference column density for difference species listed in Table 1 from surveys of cores and clumps in the Milky Way. The n_{eff} quoted can be easily scaled to another column density using Equation 13.

Since the definition of n_{eff} is arbitrary (the 1 K km/s criteria) and does not depend on a specific ratio of radiative rates to collisional depopulation rates (c.f. $\mathfrak{R} = 1$ for the definition of n_{crit}), it is seductive to use $n_{crit}^{thin, no\ bg}$ to characterize the density at which a

transition is excited as it can be analytically calculated; however, $n_{crit}^{thin,no\ bg}$ does not account for radiative trapping which can easily lower the effective critical density by more than an order of magnitude for commonly observed dense gas tracers such as $\text{HCO}^+ 1-0$, $\text{HCN } 1-0$, $\text{N}_2\text{H}^+ 1-0$, etc. The combination of $\mathfrak{R} > 1$ and radiative trapping that generate a 1 K km/s line lower n_{eff} by $\sim 1-2$ orders of magnitude relative to $n_{crit}^{thin,no\ bg}$ for many commonly observed millimeter and submillimeter lines. Furthermore, n_{eff} can account for abundance or column density differences to better differentiate the excitation density of different species than $n_{crit}^{thin,no\ bg}$ (i.e. HCO^+ vs. N_2H^+ or isotpologues vs. the main species). Overall, the effective excitation density gives a better estimate of the range of densities at which a modest (1 K km/s) molecular line can be observed; however, use of n_{eff} has the disadvantages that an appropriate column density must be determined for the observations of interest and that it is not defined for all transitions (in particular when $E_u/k \gg T_k$) and for all species (e.g. HNCO , CH_3CHO , etc.).

$n_{crit}^{thin,no\ bg}$ and n_{eff} provide only rough estimates of the densities traced and should not be over-interpreted. More sophisticated tools such as the Contribution Function (Tafalla et al. 2006) may be used to determine the various contributions to the observed line profile along the line of sight (see Pavlyuchenkov et al. 2008 for a detailed analysis of these techniques). Ultimately, if one wants to understand their observed spectra, radiative transfer modeling with publicly available codes are a fast and efficient way to determine the physical properties of a region.

Acknowledgments

I am grateful to the Max-Planck-Institut für Astronomie and Thomas Henning for hosting my Sabbatical during which this note was written. I would also like to thank John Black, Lee Mundy, Neal Evans, Henrik Beuther, Cecilia Ceccarelli, J.D. Smith, and the anonymous referee for comments and useful discussions that improved this manuscript.

REFERENCES

- Adande, G. R., & Ziurys, L. M. 2012, *ApJ*, 744, 194
- Barnes, P. J., Yonekura, Y., Fukui, Y., et al. 2011, *ApJS*, 196, 12
- Benedettini, M., Pezzuto, S., Burton, M. G., et al. 2012, *MNRAS*, 419, 238
- Blair, S. K., Magnani, L., Brand, J., & Wouterloot, J. G. A. 2008, *Astrobiology*, 8, 59
- Castor, J. I. 1970, *MNRAS*, 149, 111
- Danby, G., Flower, D. R., Valiron, P., Schilke, P., & Walmsley, C. M. 1988, *MNRAS*, 235, 229
- Daniel, F., Dubernet, M.-L., Meuwly, M., Cernicharo, J., & Pagani, L. 2005, *MNRAS*, 363, 1083
- Draine, B. T. 2011, *Physics of the Interstellar and Intergalactic Medium* by Bruce T. Draine. Princeton University Press, 2011. ISBN: 978-0-691-12214-4,
- Dumouchel, F., Faure, A., & Lique, F. 2010, *MNRAS*, 406, 2488
- Dunham, M. K., Rosolowsky, E., Evans, N. J., II, Cyganowski, C., & Urquhart, J. S. 2011, *ApJ*, 741, 110
- Ebenstein, W. L., & Muentzer, J. S. 1984, *J. Chem. Phys.*, 80, 3989
- Evans, N. J., II, Morris, G., Sato, T., & Zuckerman, B. 1975, *ApJ*, 196, 433
- Evans, N. J., II 1999, *ARA&A*, 37, 311
- Falgarone, E., Troland, T. H., Crutcher, R. M., & Paubert, G. 2008, *A&A*, 487, 247
- Flower, D. R. 1999, *MNRAS*, 305, 651
- Garrison, B. J., Lester, W. A., Jr., Miller, W. H., & Green, S. 1975, *ApJ*, 200, L175
- Gerner, T., Beuther, H., Semenov, D., et al. 2014, *A&A*, 563, AA97
- Ginsburg, A., Darling, J., Battersby, C., Zeiger, B., & Bally, J. 2011, *ApJ*, 736, 149
- Goldreich, P., & Kwan, J. 1974, *ApJ*, 189, 441
- Goorvitch, D. 1994, *ApJS*, 95, 535

- Green, S., & Thaddeus, P. 1974, *ApJ*, 191, 653
- Green, S., & Chapman, S. 1978, *ApJS*, 37, 169
- Green, S. 1986, *ApJ*, 309, 331
- Hily-Blant, P., Walmsley, M., Pineau Des Forêts, G., & Flower, D. 2010, *A&A*, 513, A41
- Hoq, S., Jackson, J. M., Foster, J. B., et al. 2013, *ApJ*, 777, 157
- Jijina, J., Myers, P. C., & Adams, F. C. 1999, *ApJS*, 125, 161
- Kauffmann, J., Bertoldi, F., Bourke, T. L., Evans, N. J., II, & Lee, C. W. 2008, *A&A*, 487, 993
- Lique, F., Spielfiedel, A., & Cernicharo, J. 2006, *A&A*, 451, 1125
- Lique, F., & Klos, J. 2011, *MNRAS*, 413, L20
- Mangum, J. G., & Wootten, A. 1993, *ApJS*, 89, 123
- Mangum, J. G., Darling, J., Menten, K. M., & Henkel, C. 2008, *ApJ*, 673, 832
- Mangum, J. G., & Shirley, Y. L. 2015, *PASP*, in press
- Miettinen, O. 2014, *A&A*, 562, AA3
- Ossenkopf, V., & Henning, T. 1994, *A&A*, 291, 943
- Osterbrock, D. E. 1989, Research supported by the University of California, John Simon Guggenheim Memorial Foundation, University of Minnesota, et al. Mill Valley, CA, University Science Books, 1989, 422 p.,
- Pavlyuchenkov, Y., Wiebe, D., Shustov, B., et al. 2008, *ApJ*, 689, 335
- Pirogov, L. E., Johansson, L. E. B., & Zinchenko, I. I. 2003, *Astronomical and Astrophysical Transactions*, 22, 33
- Plume, R., Jaffe, D. T., Evans, N. J., II, Martín-Pintado, J., & Gómez-González, J. 1997, *ApJ*, 476, 730
- Purcell, C. R., Balasubramanyam, R., Burton, M. G., et al. 2006, *MNRAS*, 367, 553
- Reiter, M., Shirley, Y. L., Wu, J., et al. 2011, *ApJS*, 195, 1
- Rosolowsky, E. W., Pineda, J. E., Foster, J. B., et al. 2008, *ApJS*, 175, 509

- Savage, C., Apponi, A. J., Ziurys, L. M., & Wyckoff, S. 2002, *ApJ*, 578, 211
- Schöier, F. L., van der Tak, F. F. S., van Dishoeck, E. F., & Black, J. H. 2005, *A&A*, 432, 369
- Scoville, N. Z., & Solomon, P. M. 1974, *ApJ*, 187, L67
- Seo, Y. M., Shirley, Y. L., Goldsmith, P., et al. 2015, *ApJ*, submitted
- Shirley, Y. L., Mason, B. S., Mangum, J. G., et al. 2011, *AJ*, 141, 39
- Shirley, Y. L., Ellsworth-Bowers, T. P., Svoboda, B., et al. 2013, *ApJS*, 209, 2
- Sobolev, V. V. 1960, Cambridge: Harvard University Press, 1960,
- Suzuki, H., Yamamoto, S., Ohishi, M., et al. 1992, *ApJ*, 392, 551
- Tafalla, M., Santiago-García, J., Myers, P. C., et al. 2006, *A&A*, 455, 577
- Townes, C. H., & Schawlow, A. L. 1975, *Microwave spectroscopy.*, by Townes, C. H.; Schawlow, A. L.. New York, NY (USA): Dover Publications, 698 p.,
- Ueda, Y., & Iwahori, J. 1986, *Journal of Molecular Spectroscopy*, 116, 191
- van der Tak, F. F. S., Black, J. H., Schöier, F. L., Jansen, D. J., & van Dishoeck, E. F. 2007, *A&A*, 468, 627
- van der Tak, F. 2011, *IAU Symposium*, 280, 449
- Wienen, M., Wyrowski, F., Schuller, F., et al. 2012, *A&A*, 544, A146
- Wiesenfeld, L., & Faure, A. 2013, *MNRAS*, 432, 2573
- Wilson, T. L., & Rood, R. 1994, *ARA&A*, 32, 191
- Yuan, Y., Esimbek, J., Zhou, J. J., et al. 2014, *Ap&SS*, 352, 521
- Zylka, R., Guesten, R., Henkel, C., & Batrla, W. 1992, *A&AS*, 96, 525

Table 1. n_{crit}^{thin} and n_{eff} for Dense Gas Tracers with Collisions with H₂

Molecule	$j \rightarrow k$	ν_{jk} (GHz)	E_j/k (K)	A_{jk} (s ⁻¹)	$n_{ph}(T_{cmb})$	$n_{crit}^{thin, no bg}(T_k) \text{ cm}^{-3}$				$\log N_{ref}$ (cm ⁻²)	$n_{eff}(T_k, N_{ref})^a \text{ cm}^{-3}$				γ_{ji}^b Ref.	
						10K	20K	50K	100K		10K	15K	20K	50K		100K
HCO ⁺	1-0	89.189	4.28	4.3E-5	0.264	6.8E+4	4.5E+4	2.9E+4	2.3E+4	14.0	9.5E+2	6.4E+2	5.3E+2	3.3E+2	2.6E+2	1
	2-1	178.375	12.84	4.1E-4	0.046	5.6E+5	4.2E+5	2.8E+5	2.2E+5		4.1E+3	2.3E+3	1.7E+3	8.9E+2	6.5E+2	
	3-2	267.558	25.68	1.5E-3	0.009	1.6E+6	1.4E+6	1.0E+6	8.1E+5		2.4E+4	1.1E+4	6.8E+3	2.6E+3	1.7E+3	
	4-3	356.734	42.80	3.6E-3	0.002	3.6E+6	3.2E+6	2.5E+6	2.0E+6		1.9E+5	5.4E+4	2.8E+4	7.2E+3	4.0E+3	
H ¹³ CO ⁺	1-0	86.754	4.16	3.9E-5	0.279	6.2E+4	4.1E+4	2.7E+4	2.0E+4	12.3	3.9E+4	2.7E+4	2.2E+4	1.4E+4	1.1E+4	1
	2-1	173.507	12.49	3.7E-4	0.050	5.1E+5	3.8E+5	2.6E+5	2.0E+5		1.7E+5	9.6E+4	7.1E+4	3.7E+4	2.6E+4	
	3-2	260.255	24.98	1.3E-3	0.011	1.5E+6	1.3E+6	9.5E+5	7.3E+5		1.3E+6	4.3E+5	2.7E+5	9.6E+4	6.2E+4	
	4-3	346.998	41.63	3.3E-3	0.002	3.4E+6	2.9E+6	2.3E+6	1.8E+6		...	2.7E+6	1.1E+6	2.7E+5	1.6E+5	
N ₂ H ⁺	1-0	93.174	4.47	3.6E-5	0.242	6.1E+4	4.1E+4	2.6E+4	2.0E+4	13.0	1.0E+4	6.7E+3	5.5E+3	3.4E+3	2.6E+3	1,2
	2-1	186.345	13.41	3.5E-4	0.040	5.0E+5	3.7E+5	2.6E+5	1.9E+5		4.6E+4	2.6E+4	1.9E+4	9.7E+3	6.9E+3	
	3-2	279.512	26.83	1.3E-3	0.007	1.4E+6	1.2E+6	9.2E+5	7.1E+5		2.6E+5	1.1E+5	6.8E+4	2.5E+4	1.6E+4	
	4-3	372.673	44.71	3.1E-3	0.001	3.2E+6	2.8E+6	2.2E+6	1.7E+6		3.0E+6	5.4E+5	2.7E+5	6.3E+4	3.4E+4	
HCN	1-0	88.632	4.25	2.4E-5	0.268	4.7E+5	3.0E+5	1.7E+5	1.1E+5	14.0	8.4E+3	5.6E+3	4.5E+3	2.6E+3	1.7E+3	3
	2-1	177.261	12.76	2.3E-4	0.047	4.1E+6	2.8E+6	1.6E+6	1.1E+6		4.1E+4	2.2E+4	1.6E+4	7.3E+3	4.5E+3	
	3-2	265.886	25.52	8.4E-4	0.010	1.4E+7	1.0E+7	5.7E+6	3.8E+6		3.0E+5	1.2E+5	7.3E+4	2.5E+4	1.3E+4	
	4-3	354.505	42.53	2.1E-3	0.002	3.0E+7	2.3E+7	1.4E+7	9.1E+6		2.1E+6	5.8E+5	3.2E+5	8.1E+4	3.7E+4	
H ¹³ CN	1-0	86.340	4.14	2.2E-5	0.282	5.3E+5	2.5E+5	1.3E+5	9.7E+4	12.3	3.5E+5	2.2E+5	1.6E+5	8.7E+4	6.5E+4	4
	2-1	172.678	12.43	2.1E-4	0.051	3.4E+6	2.2E+6	1.2E+6	9.1E+5		1.9E+6	8.6E+5	5.8E+5	1.8E+5	1.7E+5	
	3-2	259.012	24.86	7.7E-4	0.011	8.8E+6	6.6E+6	4.1E+6	3.3E+6		2.5E+7	3.8E+6	2.0E+6	6.3E+5	4.2E+5	
	4-3	345.340	41.43	1.9E-3	0.002	1.9E+7	1.5E+7	9.7E+6	7.7E+6		...	5.6E+7	1.1E+7	1.9E+6	1.1E+6	
HNC	1-0	90.664	4.35	2.7E-5	0.256	1.4E+5	1.1E+5	8.4E+4	7.0E+4	14.0	3.7E+3	2.7E+3	2.3E+3	1.7E+3	1.3E+3	3
	2-1	181.325	13.05	2.6E-4	0.043	1.3E+6	1.0E+6	8.2E+5	6.8E+5		2.0E+4	1.2E+4	9.3E+3	5.5E+3	3.9E+3	
	3-2	271.981	26.11	9.3E-4	0.009	5.1E+6	4.0E+6	3.1E+6	2.5E+6		1.6E+5	7.4E+4	4.9E+4	2.1E+4	1.2E+4	
	4-3	362.630	43.51	2.3E-3	0.002	1.3E+7	1.0E+7	7.8E+6	6.2E+6		1.4E+6	4.2E+5	2.4E+5	6.8E+4	3.4E+4	
CN	1 _{3/2} - 0 _{1/2}	113.495	5.45	1.2E-5	0.158	4.1E+5	2.4E+5	1.1E+5	6.4E+4	14.0	3.8E+4	2.3E+4	1.7E+4	7.7E+3	4.6E+3	5
	2 _{5/2} - 1 _{3/2}	226.876	16.34	1.1E-4	0.019	3.2E+6	2.2E+6	1.1E+6	6.4E+5		2.3E+5	1.1E+5	7.3E+4	2.8E+4	1.5E+4	
	3 _{7/2} - 2 _{5/2}	340.249	32.66	4.1E-4	0.003	8.3E+6	6.5E+6	3.5E+6	2.1E+6		1.8E+6	5.6E+5	3.6E+5	1.1E+5	5.1E+4	
CS	1-0	48.991	2.40	1.7E-6	0.734	1.5E+4	1.1E+4	7.8E+3	5.7E+3	13.5	8.7E+3	6.4E+3	5.4E+3	3.4E+3	2.4E+3	6
	2-1	97.981	7.10	1.7E-5	0.218	1.3E+5	1.0E+5	7.4E+4	5.5E+4		2.2E+4	1.5E+4	1.2E+4	6.9E+3	4.7E+3	
	3-2	146.969	14.10	6.1E-5	0.082	4.4E+5	3.6E+5	2.6E+5	2.0E+5		7.4E+4	4.4E+4	3.3E+4	1.6E+4	1.0E+4	
	4-3	195.954	23.50	1.5E-4	0.033	1.0E+6	8.6E+5	6.4E+5	4.8E+5		2.8E+5	1.4E+5	9.2E+4	3.6E+4	2.0E+4	
	5-4	244.936	35.30	3.0E-4	0.014	2.0E+6	1.7E+6	1.3E+6	9.5E+5		1.4E+6	4.2E+5	2.5E+5	7.6E+4	3.8E+4	
	6-5	293.912	49.40	5.2E-4	0.006	3.4E+6	2.9E+6	2.2E+6	1.6E+6		...	1.5E+6	7.1E+5	1.6E+5	7.2E+4	
	7-6	342.883	65.80	8.4E-4	0.002	5.0E+6	4.4E+6	3.4E+6	2.6E+6		...	8.8E+6	2.1E+6	3.4E+5	1.3E+5	
p-NH ₃ ^c	(1, 1)	23.694	1.14	1.7E-7	1.940	2.0E+3	1.8E+3	1.2E+3	8.7E+2	14.3	9.3E+2	7.9E+2	7.6E+2	7.4E+2	7.3E+2	7
	(2, 2)	23.723	42.32	2.3E-7	1.937	1.6E+3	1.5E+3	1.4E+3	1.1E+3		...	1.6E+4	3.9E+3	1.3E+3	9.4E+2	
	2 ₁ ⁺ - 1 ₁ ⁺	1168.452	57.21	1.2E-2	0.000	1.2E+8	1.1E+8	9.0E+7	6.7E+7		...	4.8E+7	8.6E+6	1.4E+6	8.2E+5	
o-NH ₃ ^c	2 ₁ ⁺ - 1 ₁ ⁺	1215.245	58.32	1.4E-2	0.000	1.4E+8	1.2E+8	1.0E+8	7.5E+7		...	7.2E+7	1.0E+7	1.6E+6	8.9E+5	
	(3, 3)	23.870	123.54	2.6E-7	1.923	1.5E+3	1.5E+3	1.4E+3	1.2E+3	14.6	4.0E+2	1.7E+2	7
	1 ₀ - 0 ₀	572.498	27.48	1.6E-3	0.000	4.0E+7	3.1E+7	1.7E+7	9.9E+6		6.2E+5	1.5E+5	8.4E+4	3.1E+4	2.5E+4	
p-H ₂ CO	2 ₀ - 1 ₀	1214.859	85.78	1.8E-2	0.000	2.1E+8	1.9E+8	1.6E+8	1.1E+8		...	4.2E+7	4.4E+6	5.2E+5	3.0E+5	
	1 _{0,1} - 0 _{0,0}	72.838	3.50	8.2E-6	0.386	4.5E+4	2.8E+4	1.8E+4	1.4E+4	12.7	5.0E+4	3.2E+4	2.6E+4	1.9E+4	1.8E+4	8
	2 _{0,2} - 1 _{0,1}	145.603	10.50	7.8E-5	0.084	3.4E+5	2.5E+5	1.7E+5	1.3E+5		1.5E+5	8.2E+4	6.3E+4	4.3E+4	4.0E+4	
	3 _{0,3} - 2 _{0,2}	218.222	21.00	2.8E-4	0.022	9.7E+5	7.8E+5	5.7E+5	4.7E+5		7.7E+5	2.9E+5	2.0E+5	1.2E+5	1.1E+5	
	4 _{0,4} - 3 _{0,3}	290.623	34.90	6.9E-4	0.006	1.9E+6	1.7E+6	1.3E+6	1.1E+6		...	1.5E+6	7.3E+5	3.1E+5	2.6E+5	
	5 _{0,5} - 4 _{0,4}	362.736	52.30	1.4E-3	0.002	3.6E+6	3.1E+6	2.6E+6	2.2E+6		3.8E+6	8.0E+5	5.9E+5	
o-H ₂ CO	1 _{1,0} - 1 _{1,1}	4.830	15.40	3.6E-9	11.310	1.3E+1	1.0E+1	7.6E+0	6.1E+0	13.0	8
	2 _{1,1} - 2 _{1,2}	14.488	22.60	3.2E-8	3.456	1.1E+2	8.7E+1	6.5E+1	5.3E+1		
	2 _{1,2} - 1 _{1,1}	140.840	21.90	5.3E-5	0.092	1.5E+5	1.3E+5	1.1E+5	9.0E+4		9.5E+4	5.9E+4	4.6E+4	2.6E+4	2.0E+4	
	2 _{1,1} - 1 _{1,0}	150.498	22.60	6.5E-5	0.077	2.2E+5	1.8E+5	1.3E+5	1.1E+5		1.7E+5	1.1E+5	8.6E+4	4.9E+4	3.5E+4	

Table 1—Continued

Molecule	$j \rightarrow k$	ν_{jk} (GHz)	E_j/k (K)	A_{jk} (s^{-1})	$n_{ph}(T_{cmb})$	$n_{crit}^{thin, no\ bg}(T_k) \text{ cm}^{-3}$				$\log N_{ref}$ (cm^{-2})	$n_{eff}(T_k, N_{ref})^a \text{ cm}^{-3}$					γ_{ji}^b Ref.
						10K	20K	50K	100K		10K	15K	20K	50K	100K	
HC ₃ N ^d	3 _{1,3} – 2 _{1,2}	211.211	32.10	2.3E-4	0.025	5.6E+5	5.1E+5	4.3E+5	3.8E+5		4.6E+5	2.0E+5	1.4E+5	6.3E+4	4.9E+4	
	3 _{1,2} – 2 _{1,1}	225.698	33.40	2.8E-4	0.019	8.4E+5	7.0E+5	5.5E+5	4.6E+5		8.9E+5	3.8E+5	2.6E+5	1.3E+5	9.0E+4	
	4 _{1,4} – 3 _{1,3}	281.527	45.60	5.9E-4	0.007	1.4E+6	1.3E+6	1.1E+6	9.8E+5		2.9E+7	9.9E+5	5.1E+5	1.7E+5	1.2E+5	
	4 _{1,3} – 3 _{1,2}	300.837	47.90	7.2E-4	0.005	2.0E+6	1.7E+6	1.4E+6	1.2E+6		...	1.9E+6	9.6E+5	3.3E+5	2.2E+5	
	5 _{1,5} – 4 _{1,4}	351.769	62.50	1.2E-3	0.002	2.8E+6	2.6E+6	2.2E+6	2.0E+6		...	1.7E+7	2.3E+6	4.3E+5	2.6E+5	
	2 – 1	18.196	1.31	3.9E-7	2.659	9.7E+2	7.5E+2	5.3E+2	4.1E+2	13.0	5.9E+3	3.1E+3	2.3E+3	1.0E+3	8.4E+2	9
	3 – 2	27.294	2.62	1.4E-6	1.628	3.5E+3	2.6E+3	1.8E+3	1.6E+3		4.7E+3	3.0E+3	2.3E+3	1.1E+3	8.7E+2	
	4 – 3	36.392	4.37	3.5E-6	1.119	9.1E+3	6.8E+3	4.7E+3	3.7E+3		6.2E+3	3.8E+3	2.8E+3	1.5E+3	1.1E+3	
	5 – 4	45.490	6.55	6.9E-6	0.819	1.8E+4	1.3E+4	9.6E+3	7.2E+3		9.6E+3	5.6E+3	4.1E+3	2.1E+3	1.5E+3	
	8 – 7	72.784	15.72	2.9E-5	0.387	7.7E+4	5.9E+4	4.1E+4	3.1E+4		5.3E+4	2.5E+4	1.6E+4	6.4E+3	4.0E+3	
	9 – 8	81.881	19.65	4.2E-5	0.312	1.1E+5	8.3E+4	6.2E+4	4.6E+4		1.1E+5	4.2E+4	2.6E+4	9.4E+3	5.7E+3	
	10 – 9	90.979	24.01	5.8E-5	0.254	1.6E+5	1.2E+5	8.2E+4	6.3E+4		4.3E+5	7.2E+4	4.3E+4	1.4E+4	8.1E+3	
	11 – 10	100.076	28.82	7.8E-5	0.209	2.0E+5	1.6E+5	1.1E+5	9.2E+4		...	1.6E+5	7.0E+4	2.0E+4	1.1E+4	
	12 – 11	109.173	34.06	1.0E-4	0.173	2.8E+5	2.1E+5	1.5E+5	1.1E+5		...	2.3E+5	1.1E+5	2.8E+4	1.6E+4	
	14 – 13	127.367	45.85	1.6E-4	0.120	3.4E+5	3.1E+5	2.5E+5	1.9E+5		3.8E+5	5.7E+4	3.0E+4	
15 – 14	136.464	52.40	2.0E-4	0.100	5.5E+5	4.3E+5	3.1E+5	2.4E+5		8.2E+5	8.1E+4	4.2E+4		
CH ₃ CN ^e	4 ₀ – 3 ₀	73.590	8.83	3.2E-5	0.379	1.2E+5	8.6E+4	5.4E+4	4.1E+4	13.0	5.2E+4	4.0E+4	3.7E+4	2.5E+4	2.5E+4	10
	5 ₀ – 4 ₀	91.987	13.24	6.3E-5	0.249	2.5E+5	1.7E+5	1.1E+5	8.3E+4		1.2E+5	8.4E+4	7.4E+4	4.3E+4	4.0E+4	
	6 ₀ – 5 ₀	110.384	18.54	1.1E-4	0.169	4.5E+5	3.1E+5	1.9E+5	1.5E+5		3.2E+5	1.8E+5	1.5E+5	7.6E+4	6.5E+4	
	7 ₀ – 6 ₀	128.779	24.72	1.8E-4	0.117	7.3E+5	5.1E+5	3.1E+5	2.4E+5		1.0E+6	4.2E+5	3.1E+5	1.4E+5	1.1E+5	
	8 ₀ – 7 ₀	147.175	31.79	2.7E-4	0.082	1.1E+6	7.7E+5	4.8E+5	3.6E+5		8.8E+6	1.0E+6	6.5E+5	2.3E+5	1.7E+5	
9 ₀ – 8 ₀	165.569	39.73	3.8E-4	0.058	1.6E+6	1.1E+6	6.9E+5	5.2E+5		...	3.1E+6	1.4E+6	4.0E+5	2.8E+5		

^aThe effective excitation density may be converted to another column density using $n_{eff}(T_k, N) = n_{eff}(T_k, N_{ref}) \frac{N_{ref}}{N}$ for $n_{eff} \lesssim 5 \times 10^6 \text{ cm}^{-3}$. Logarithmic interpolation should be used to convert n_{eff} to other T_k .

^bThe collisional rates for collisions with H₂ in $\text{cm}^{-3} \text{ s}^{-1}$ were obtained from the Leiden LAMDA database (August 2014). The original references for the collision rates are: 1. Flower et al. 1999, 2. Daniel et al. 2005, 3. Dumouchel et al. 2010, 4. Green & Thaddeus 1974, 5. Lique et al. 2011, 6. Lique et al. 2006, 7. Danby et al. 1988, 8. Wiesenfeld & Faure 2013, 9. Green & Chapman 1978, 10. Green 1986. Rates calculated for collisions with He are scaled in the LAMDA database by the reduced mass (1.36) to convert to approximate rates for collisions with H₂. Collision rates with hyperfine transitions collapsed were used for the calculations in this table.

^c $n_{crit}^{thin, no\ bg}$ was logarithmically extrapolated to $T_k = 10\text{K}$ since the lowest T_k calculated in the collision rate file was 15K.

^d $n_{crit}^{thin, no\ bg}$ was logarithmically extrapolated to $T_k = 100\text{K}$ since the highest T_k calculated in the collision rate file was 80K.

^e $n_{crit}^{thin, no\ bg}$ was logarithmically extrapolated to $T_k = 10\text{K}$ since the lowest T_k calculated in the collision rate file was 20K.